PERGAMON

International Journal of Solids and Structures 38 (2001) 7181–7196

INTERNATIONAL JOURNAL OF SOLIDS and STRUCTURES

www.elsevier.com/locate/ijsolstr

Mechanical behavior of a three-dimensional truss material

J.C. Wallach [a], L.J. Gibson [b,*]

[a] *Department of Mechanical Engineering, Massachusetts Institute of Technology, 77, Massachusetts Avenue 8-135, Cambridge, MA 02139, USA*

[b] *Department of Materials Science and Engineering, Massachusetts Institute of Technology, 77, Massachusetts Avenue 8-135, Cambridge, MA 02139, USA*

Received 2 February 2000

Abstract

A variety of novel manufacturing techniques can be used to make materials with a periodic, three-dimensional (3D) truss-like structure. The high stiffness per unit weight of such structures makes them attractive for use in sandwich panels. In this paper, we analyze the elastic moduli as well as the uniaxial and shear strengths of one particular geometry of 3D truss material as a function of the aspect ratio of the unit cell. The analysis gives a good description of the measured properties. © 2001 Elsevier Science Ltd. All rights reserved.

Keywords: Truss structures; Light weight metal structures; Cellular structures; Lattice block

1. Introduction

A typical three-dimensional (3D) truss material made of a cast aluminum alloy is shown in Fig. 1. The structure has a periodic unit cell with fully triangulated members. A variety of manufacturing techniques are available for producing such materials. The top lattice, the bottom lattice and the core can be separately injection molded with a polymer, assembled to form a complete structure, and then used as a mold for investment casting if a metallic material is desired. The top lattice, bottom lattice and core can also be made separately from a thin layer of silver, assembled and then electroplated with another metal, such as nickel. The silver lattices are made as follows. All three layers (the top lattice, the bottom lattice and the core) are made as flat grids. A master of each of the three patterns is made of an elastomer using conventional photolithography. The master is then used to stamp a self-assembled monolayer onto a glass slide coated with a 50 nm thick layer of silver. The silver which is not stamped with the self-assembled monolayer is removed by chemical etching. The core layer is then folded to obtain the 3D structure, the three layers are hand assembled and the resulting silver truss material is then electroplated with nickel. 3D printing techniques can be used to build up the structure, layer by layer. Stereolithography techniques can be used to

* Corresponding author. Tel.: +1-617-253-7107; fax: +1-617-258-6275.
E-mail address: ljgibson@mit.edu (L.J. Gibson).

0020-7683/01/$ - see front matter
PII: S0020-7683(00)00400-5

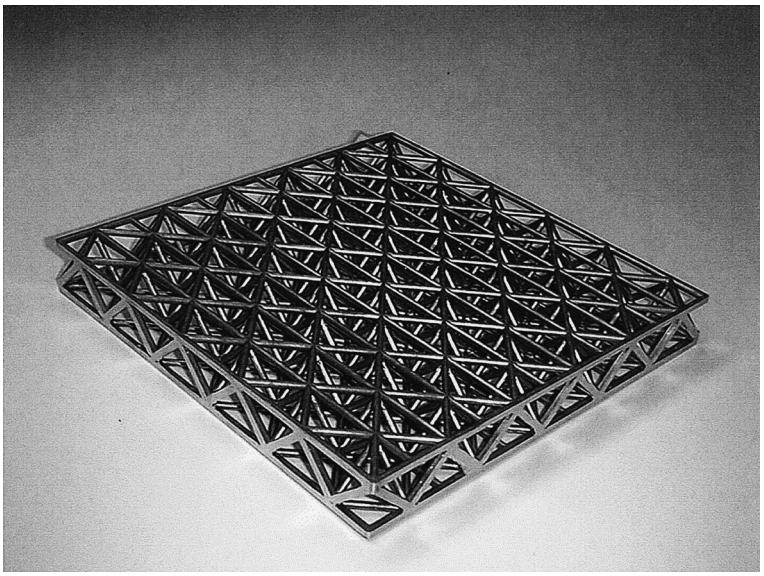

Fig. 1. Photograph of 3D truss material made from an aluminum casting alloy.

cure sequential layers of light-sensitive resin with a laser. The dimensions of the unit cell range from one to tens of millimeters.

The fully triangulated, 3D truss structure induces axial forces in the individual members, so that it is expected to have a high specific stiffness and strength, making it attractive for use in structural sandwich panels. In contrast, metallic foams deform primarily by cell wall bending, reducing their effectiveness in structural applications.

In this paper, we analyze the elastic moduli as well as the uniaxial and shear strengths of one particular geometry of 3D truss material, shown in Fig. 1, as a function of the aspect ratio of the unit cell. The properties of the material are measured using conventional techniques. The analysis gives a good description of the uniaxial and shear response of the 3D truss material.

2. Modeling

We consider an infinite plane of repeating unit cells in the x and y directions. The material has a depth of a single cell in the z direction. The periodic unit cell for the material is shown in Fig. 2. Members located on the sides of the unit cell are shared between two adjacent cells, so that the cross-sectional area of these members is half that of the remaining members. The relative density of the structure (the density of the truss material divided by that of the solid from which it is made) is given by:

$$\frac{\rho^*}{\rho_s} = \frac{4 + 4\sqrt{2} + 8\sqrt{\mathrm{AR}^2 + (1/4)}}{\mathrm{AR}} \pi \left(\frac{r^2}{b^2}\right)$$

where $\mathrm{AR} = h/b$ is the aspect ratio of the unit cell, r is the radius of a single member, and b is the cell base.

The unit cell has two planes of symmetry passing through the middle of the cell (the x–z and the y–z planes). The presence of the symmetry planes requires that normal stress and strain be independent from

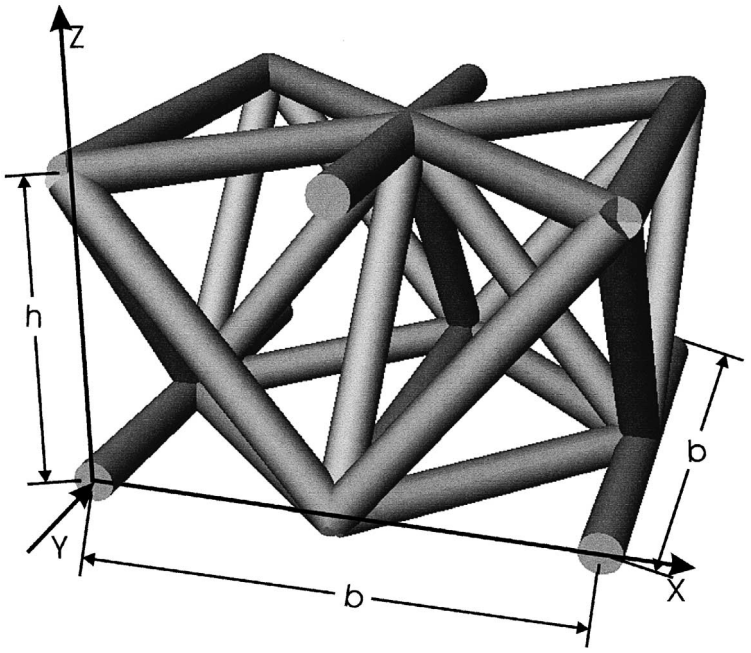

Fig. 2. Unit cell of the infinite planar truss material, one cell high.

shear stress and strain, giving the material orthotropic symmetry. The linear elastic behavior can be described by nine independent elastic constants, as shown below:

$$\begin{bmatrix} \varepsilon_1 \\ \varepsilon_2 \\ \varepsilon_3 \\ \gamma_4 \\ \gamma_5 \\ \gamma_6 \end{bmatrix} = \begin{bmatrix} \frac{1}{E_1} & -\frac{\nu_{12}}{E_2} & -\frac{\nu_{13}}{E_3} & 0 & 0 & 0 \\ -\frac{\nu_{21}}{E_1} & \frac{1}{E_2} & -\frac{\nu_{23}}{E_3} & 0 & 0 & 0 \\ -\frac{\nu_{31}}{E_3} & -\frac{\nu_{32}}{E_3} & \frac{1}{E_3} & 0 & 0 & 0 \\ 0 & 0 & 0 & \frac{1}{G_4} & 0 & 0 \\ 0 & 0 & 0 & 0 & \frac{1}{G_5} & 0 \\ 0 & 0 & 0 & 0 & 0 & \frac{1}{G_6} \end{bmatrix} \begin{bmatrix} \sigma_1 \\ \sigma_2 \\ \sigma_3 \\ \sigma_4 \\ \sigma_5 \\ \sigma_6 \end{bmatrix}$$

The Poisson ratios, ν_{ij}, are defined for loading in the j direction as follows:

$$\nu_{ij} = -\frac{\varepsilon_i}{\varepsilon_j}.$$

The mechanical response of an infinite plane of the truss material was calculated from that of the unit cell. Since the material is periodic before deformation, it must also be periodic after deformation, requiring periodic boundary conditions. For loading by a normal stress, it is sufficient to constrain the unit cell faces to remain flat, parallel and mutually perpendicular. For loading by a shear stress, we observe that each shear mode is independent: for example x–z shear is independent from y–z shear. Consequently, we model shear by imposing a single shear mode and then calculating the resultant stress. This approach leads to individual sets of boundary conditions for shearing in the x–z, y–z, and x–y planes. The core struts, those lying between the upper and lower faces, are identical in the x and y directions. It follows that the z–y and z–x shear modes exhibit identical properties. For example, consider x–z shear imposed by fixing the lower face and moving the upper face in the x direction. Only struts in the core deform, while struts on both faces

remain unstressed. If instead we had displaced the upper face in the y direction the situation would be the same: only the core members would be stressed. Since the core struts exhibit 90° rotational symmetry, z–x and z–y shear response must be the same.

The analysis was done numerically with the aid of a microcomputer using two methods. In the first method we wrote a truss-analysis program in MATLAB (The MathWorks, Inc., Natick, Massachusetts) based on matrix methods outlined in Weaver and Gere (1990). The program offered flexibility for parametric analysis and data manipulation, but performed only linear elastic analyses. The second method employed a commercial finite element code, ABAQUS (Hibbitt, Karlsson, and Sorenson, Inc., Pawtucket, Rhode Island). This approach confirmed selected results from the MATLAB analyses and allowed us to extend the analysis to include nonlinear effects such as material yield and large deformation.

In both methods, the elastic moduli of the material were analyzed by treating each member of the unit cell as a linear spring. Each end of the spring contains a single node where boundary conditions and/or interconnections may be applied. In the matrix analysis the springs were modeled directly while in the finite element analysis the members were modeled with truss elements, which are themselves linear springs. The appropriate force–displacement relationship is:

$$F = \frac{AE}{L}(x_2 - x_1)$$

where A is the cross-sectional area, E is Young's modulus, L is the element length, and x_1 and x_2 are displacements at the nodes.

In the finite element analysis, the solid material was modeled as elastic, elastic-strain hardening, or elastic-strain hardening failure, depending on the analysis. Simple elastic analyses used a Young's modulus $E = 69$ GPa. Elastic-strain hardening analyses used a piecewise linear fit to experimental data for the uniaxial tensile stress–strain curve for the solid which was measured as part of the experimental procedure, described below.

Boundary conditions for the analyses were specified by dictating conditions for deformation in the x, y, and z directions at each node. The node numbering and loading arrangement used to analyze x direction deformation are shown in Fig. 3. Many nodes are left free in one or more directions. Some nodes are restrained so that they cannot move: for example all the nodes on the bottom face are restrained the z direction. Some nodes have imposed displacements: for example node 3, on the right side, is displaced in the negative x direction. Many nodes are linked to other nodes, requiring that both nodes displace the same amount: for example nodes 5, 8, 11, and 15 are linked to node 3 in the x direction. Linking greatly simplifies periodic boundary conditions: for example all the nodes on the front face $\{1, 2, 3, 9, 10, 11\}$ move together in the y direction, so nodes $\{2, 3, 9, 10, 11\}$ are linked to node 1 in the y direction. If node 1 is free in the y direction, the entire face can move but all the nodes must remain planar and the face will not rotate. [1]

Modeling the members of the unit cell as simple truss members implies that the joints are pinned and the contribution of bending moments in the actual structure is neglected. The 3D truss material is fully triangulated, meaning that it will support loads even if bending moments are neglected. To estimate the error associated with using truss elements we considered a very simple triangulated structure: an isosceles right triangle with the inclined members at 45° to the horizontal member and with dimensions similar to those of the members in the 3D truss material; the inclined members had a length to thickness ratio, L/t of 8.5. The triangle was analyzed using ABAQUS, once with truss elements, neglecting the contribution of bending moments, and then again with beam elements, including the contribution of bending moments. A dis-

[1] The linking procedure was used in the matrix analysis and with ABAQUS. The matrix analysis equations outlined in Weaver and Gere (1990) had to be modified considerably to include linking. Linking was implemented in ABAQUS using the equation feature, which can force one nodal degree of freedom to follow another.

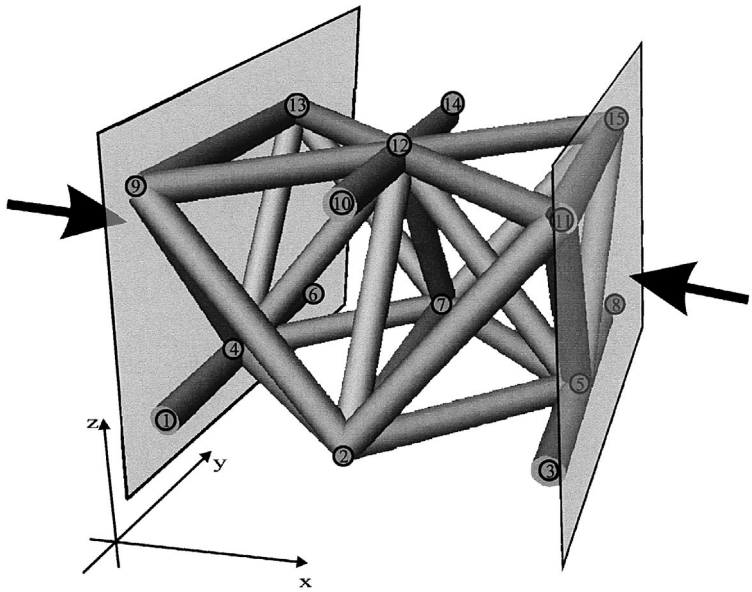

Fig. 3. Boundary conditions for the analysis of the unit cell for loading in the x direction.

placement was applied to the vertex of the triangle and resultant forces were calculated. The results indicate that the error associated with neglecting bending moments is approximately 1.4%.

The unit cell model was used to calculate the properties of an infinite planar array of material one cell high. The mechanical properties of the truss material were measured on specimens of finite size with a relatively small number of unit cells. The stiffness and strength of finite size specimens are expected to be greater than those for the infinite array as the outer edge members of the finite specimens are of full, rather than half, thickness. The effect of specimen size on the calculated properties was analyzed by modeling the finite structures, including all the elements and nodes, to represent the entire structure. The models were assembled using a script which creates a model with any integer number of unit cells along each side. This analysis was used both to characterize the effect of specimen size on the calculated properties of the truss material and to compare the results of the models with the measured properties.

In the actual truss material, the inner members that extend between the upper and lower faces meet at a point below (or above) the upper (or lower) faces. The inner strut offset, d, was measured to be 2.4 mm (Fig. 4). A more detailed model was developed to include inner strut offset. The model included additional nodes at the correct endpoints of the inner struts. These were rigidly connected to nodes on the faces using the equation feature of ABAQUS: x, y, and z translation was constrained to follow the translation of nearby face nodes.

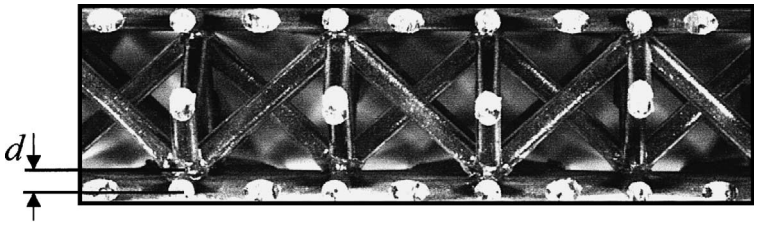

Fig. 4. Photograph of the truss material, showing the inner strut offset, d.

The actual structure appears to be regular and we could not measure any variation in cell size (with resolution 0.2 mm). In a perfect structure, multiple members experience the same stress and should, theoretically, fail at the same load. In practice, tension tests produced a significant variation in the failure strain of the members: the average was 1.95% with a standard deviation of 1.25%. The models were modified by introducing a random perturbation to the node locations, simulating random variation within the individual struts, and guaranteeing that members would fail individually. Perturbations were applied to the x, y, and z coordinates; each was chosen from a uniform distribution with mean 0 and range ± 2.5 mm. Elastic and strength properties reported below represent a perfect structure; the perturbed results are reported afterward for comparison.

Finally, the effect of the aspect ratio, h/b, of the unit cell on the elastic moduli and uniaxial strength of the truss material were calculated using the infinite planar model. The elastic properties were calculated for a perfect model neglecting inner strut offset. The strength properties were calculated for a perfect model including inner strut offset. The aspect ratio of the material tested in this study was 0.62.

3. Modeling results

The complete set of nine independent elastic moduli of the infinite planar array of the truss material, neglecting inner strut offset, are plotted against aspect ratio, h/b, in Fig. 5. The truss structure induces axial forces in the members, so that the effective Young's moduli and shear moduli vary linearly with relative density, ρ^*/ρ_s. The effective moduli can then be written as:

$$\frac{E^*}{E_s} = C_1\left(\frac{\rho^*}{\rho_s}\right) \quad \text{or} \quad \frac{G^*}{E_s} = C_2\left(\frac{\rho^*}{\rho_s}\right).$$

In Fig. 5, the Young's moduli and shear moduli are normalized by Young's modulus of the solid, E_s, and the relative density, ρ^*/ρ_s, of the truss material so that the value of the constants C_1 and C_2 are given by the ordinate of the plot. It is observed that G_{xz} and G_{yz} coincide, as expected. Three Poisson's ratios are plotted in Fig. 5; the three that have been omitted can be calculated using the reciprocal relation $E_i v_{ij} = E_j v_{ji}$.

The uniaxial strength of the ideal infinite planar truss material is plotted against aspect ratio, h/b, in Fig. 6. The strengths have been normalized by the yield strength of the solid, σ^*_{ys} and by the relative density, ρ^*/ρ_s of the truss material. Strength is defined as the peak stress. The model includes the inner strut offset refinement ($d = 2.4$ mm), but not the random perturbations in the nodes. For small aspect ratios the offset distance, d, becomes significant compared to the unit cell height so that the results are meaningful only for aspect ratios greater than about 0.4.

The effect of specimen size on the calculated Young's moduli of square tiles of the perfect planar truss material is shown in Fig. 7, neglecting inner strut offset. As expected, the moduli decrease as the specimen size increases, due to the effect of the edge members of full, rather than half, thickness in the finite size specimens. The effect is most pronounced for loading in the x direction; in this case, it becomes significant for specimens with fewer than six unit cells.

4. Experimental methods

The aluminum alloy truss material was obtained in square tiles 214×214 mm^2 (5.5×5.5 unit cells) (Jamcorp, Wilmington, MA). The composition of the aluminum alloy was measured using wavelength dispersive spectrometry (Jeol JXA-733 Superprobe, Peabody, MA). The truss members were cylindrical, with radius $r = 1.59$ mm. The unit cell had a height, $h = 23.50$ mm and a base width, $b = 38.10$ mm. Specimens for mechanical testing were cut from these tiles with a band saw such that they were slightly oversized, with portions of struts extending beyond the load-carrying cells.

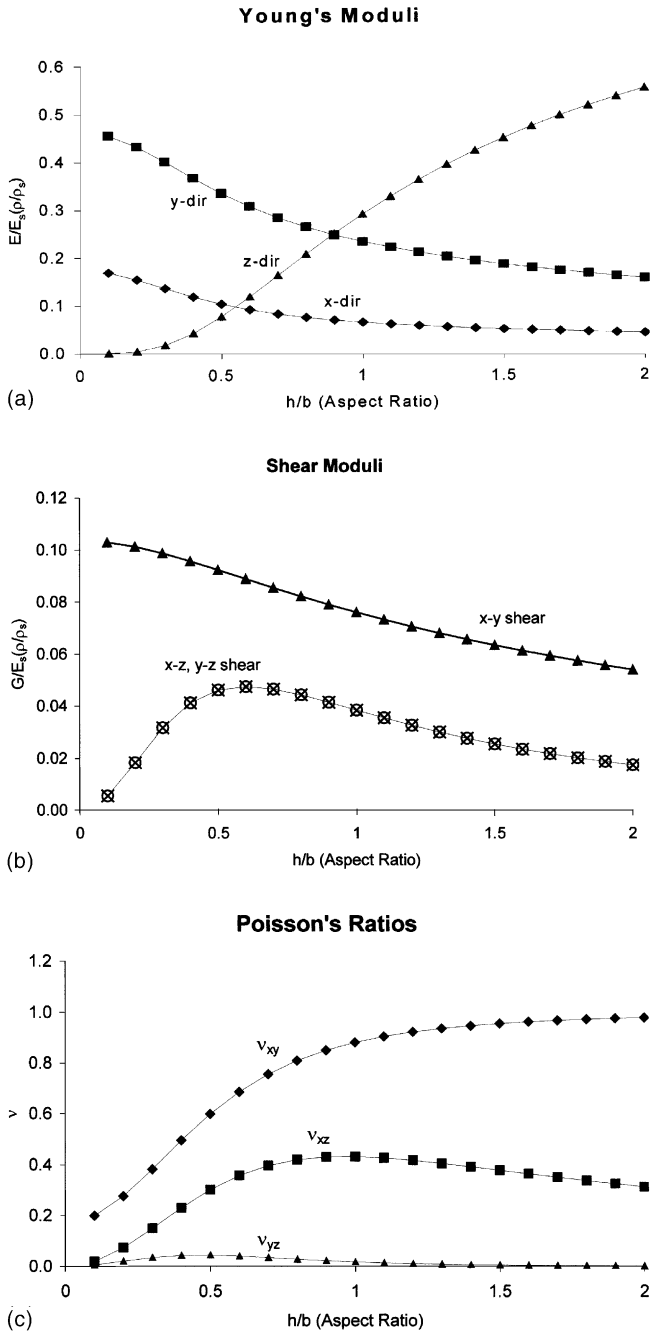

Fig. 5. The calculated elastic moduli of the infinite planar truss material plotted as a function of the aspect ratio, h/b, of the unit cell. (a) Young's moduli, (b) the shear moduli and (c) Poisson's ratios. Young's moduli and the shear moduli are normalized by Young's modulus of the solid strut material and the relative density of the truss material.

The uniaxial tensile stress–strain curve of the solid from which truss material was made was first measured. Individual struts were cut from a tile and machined into waisted specimens suitable for tension

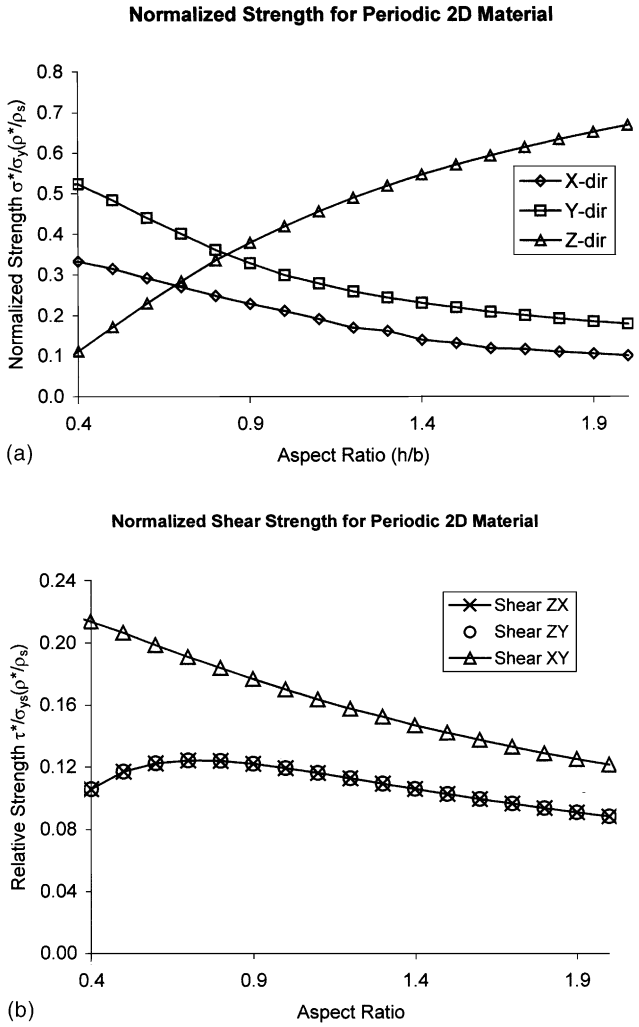

Fig. 6. The calculated uniaxial strength of the infinite planar truss material plotted as a function of the aspect ratio, h/b, of the unit cell. The strength is normalized by the yield strength of the solid strut material and the relative density of the truss material.

tests. The finished specimens had a waisted diameter of 2.54 mm and waisted length of 15.2 mm. They were loaded in tension in a mechanical testing machine (Model 4201, Instron Corp., Canton, MA) while measuring force with a load cell and strain with an extensometer of gauge length 12.5 mm. Seven specimens of the solid material were tested.

The uniaxial compressive stress–strain curve of the solid was also measured. Individual struts were cut into 14 mm long cylinders and tested in compression between steel platens (Model 4201, Instron Corp., Canton, MA). Force was measured with a load cell and displacement was measured with an LVDT (050 MHR, Lucas Shaevitz, Hampton, VA). Four specimens were tested in this manner.

The uniaxial compressive response of the truss material was measured directly on specimens cut from the tiles. For loading in the x and y directions, the specimens were cut to be five cells long in the compression direction, and one cell long in the perpendicular direction. For loading in the z direction, the specimens were constrained to be only one cell high in the loading direction as this was the height of the tiles obtained

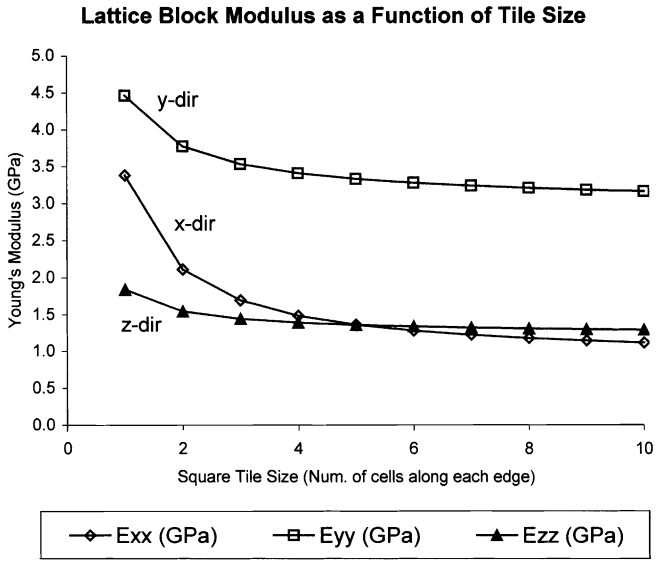

Fig. 7. The calculated Young's moduli of the truss material plotted against normalized specimen size, L/b.

from the manufacturer. Young's modulus in the z direction was measured on small specimens (1.5 cells $\times$ 2 cells in area). All of these specimens were tested using a 25 kip capacity Instron testing machine (model 1321, Instron Corp., Canton, MA). However the capacity of this machine was insufficient to measure the strength of the truss material in the z direction. Additional tests were performed on a 100 kip capacity machine (MTS Test Frame 311.21, Minneapolis, MN) using larger specimens (2 cells $\times$ 4 cells). The strength of the truss material in the z direction was measured from these tests. We were unable to obtain reliable displacement data from the latter tests because the platens lacked mounting points for an LVDT, so a reliable stress–strain curve was not obtained. In all cases the specimens were tested in compression between steel platens. Platens on the 25 kip machine were 25 mm thick, and platens on the 100 kip machine were 50 mm thick. Force was measured with a load cell and displacement was measured with LVDTs mounted directly to the platens (for the 25 kip machine). Three specimens were tested in compression for each of the x, and y directions, and two were tested for each of the z direction experiments.

The shear response of the truss material was measured in accordance with ASTM standard C273-61 (1994). Due to sample size requirements, it was possible only to measure the shear response in the z–x and z–y planes. A sample of the truss material of dimensions 12.75 in $\times$ 2.25 in was bonded to 0.5 in. thick aluminum plates using the structural adhesive FM-123-2 (Cytec, Harve de Grace, MD). The assembly was cured in an autoclave at 107°C and 0.28 MPa for 2 h. Tests were performed by pulling the sample in tension, along the diagonal of the specimen. Displacement was measured with two high-precision LVDTs (050 MHR, Lucas Shaevitz, Hampton, VA) mounted directly on rigid plates attached to the specimen. Force was again measured with a load cell. Four specimens were tested in shear: two in the z–x plane and two in the z–y plane.

5. Experimental results

The composition of the aluminum alloy was found to be 95% Al, 4% Si, and 0.2% Fe, with traces of Cu and Zn. This composition is similar to alloy 443, a casting alloy with 4.5–6.0% Si. Since the truss material is manufactured through investment casting, we expect the aluminum to be a casting alloy.

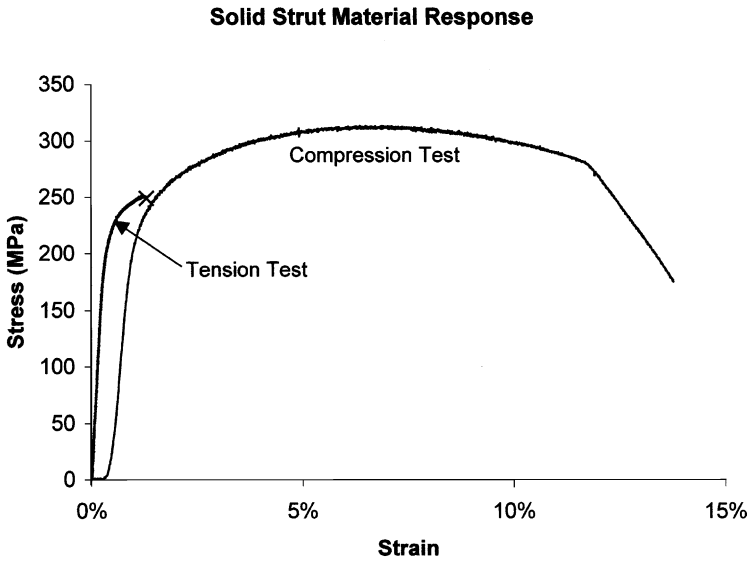

Fig. 8. Uniaxial tensile and compressive stress–strain curve for the solid strut material.

Typical uniaxial tensile and compressive stress–strain curves for the solid aluminum alloy specimens are shown in Fig. 8. The tensile curve exhibits mild yielding and then brittle fracture, perhaps related to a void nucleation and growth mechanism. The compression curve exhibits yielding, strain hardening, and eventually a decrease in load corresponding to specimen buckling. Young's modulus, E_s, is 69 GPa and the 0.2% offset yield strength, σ^*_{ys}, is 224 MPa. The strain to failure for the tensile stress–strain curve shown is 1.3%; values varied from 0.4% to 4.0% among the seven tests. The low ductility is typical of brittle aluminum casting alloys. Alloys 443.0-F, B443.0-F, and C443.0-F have yield strengths of 55–110 MPa, tensile strengths of 130–230 MPa, and elongation to failure of 8–10% (Davis, 1996). The tensile stress–strain curve shown in Fig. 8 was used for the elastic-strain hardening failure analyses since it gives a conservative estimate of the failure strain.

Typical stress–strain curves for loading the truss material in the x, y and z directions are shown in Fig. 9. For loading in the x and y directions, the curves initially exhibit an increasing slope, corresponding to the specimens deforming slightly to contact the loading plates at each point across the loading surface. Subsequent loading produces a linear stress–strain relationship. Eventually the specimens begin to yield and the slope of the curves decreases slowly. When the first member fails the stress drops instantaneously. This and subsequent member failures are accompanied by audible pings. The specimens were partially unloaded for elastic modulus calculations; the unloading portions of the stress–strain curves overlap the loading curves.

The properties of the truss material in the z direction were measured in two sets of tests due to difficulties with the capacity of the testing machines and with measuring displacements. The first set gave the linear elastic portion of the stress–strain curve, shown in Fig. 9, while the second gave the failure stress. The average value of the compressive strength of the truss material in the z direction is 9.01 MPa.

Failure in specimens loaded in the x direction corresponded to the sudden fracture of individual members loaded in tension (Fig. 10a). Failure in specimens loaded in the y direction corresponded to buckling of individual top- and bottom-lattice members loaded in compression (Fig. 10b). Failure in specimens loaded in the z direction corresponded to tensile fracture in top and bottom members and buckling in core members (Fig. 10c).

A typical stress–strain curve for loading in shear in the z–x plane (equivalent to the z–y plane) is shown in Fig. 11. The curve is initially linear and gives, on average, a shear modulus of 1.17 GPa. The modulus

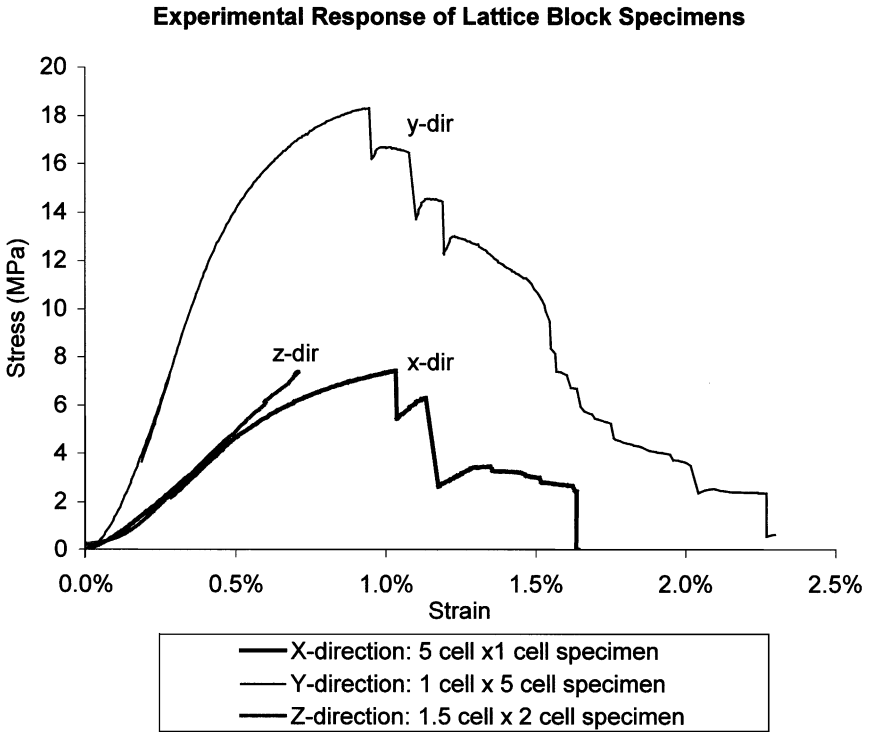

Fig. 9. Measured uniaxial compressive stress–strain curves for the truss material for loading in the x, y and z directions.

was calculated from partial unloading curves, which happen to overlap the loading curves exactly. The measured moduli had a standard deviation of 9%. After loading the stress dips slightly, rises again, and then declines slowly, corresponding to debonding between the specimen and the aluminum plates. As a result of debonding, we were unable to measure the yield and failure response in shear.

6. Discussion

The predicted and experimental data for elastic properties are compared in Table 1. The calculated values are the results obtained by modeling the exact geometry of the test. For example, the x direction compression tests used 5 cells $\times$ 1 cell specimens, so the calculated value for x direction modulus is obtained by modeling a 5 cells $\times$ 1 cell structure. The calculations used perfect models (no node perturbations) and included inner strut offset. Agreement between the experimental data and model results is good. The discrepancy between experiment and model for E_x, E_y, E_z, and G_{xz} are -15%, $+3\%$, $+7\%$, and -27%, respectively. Elastic properties for the infinite planar array and for an infinite truss material in 3D are also included in Table 1. The moduli of the finite material are higher than those of infinite material, due to the full, rather than half, thickness of the members at the edges. The 3D periodic calculations assumed a material with the same unit cell dimensions and the same member diameter as the tested specimens. This 3D periodic material has a relative density 9.89%, well below 14.2% for the two dimensional (2D) periodic material. The lower relative density occurs because the top and bottom faces contain half-thickness members, rather than the full-thickness members in the 2D periodic material.

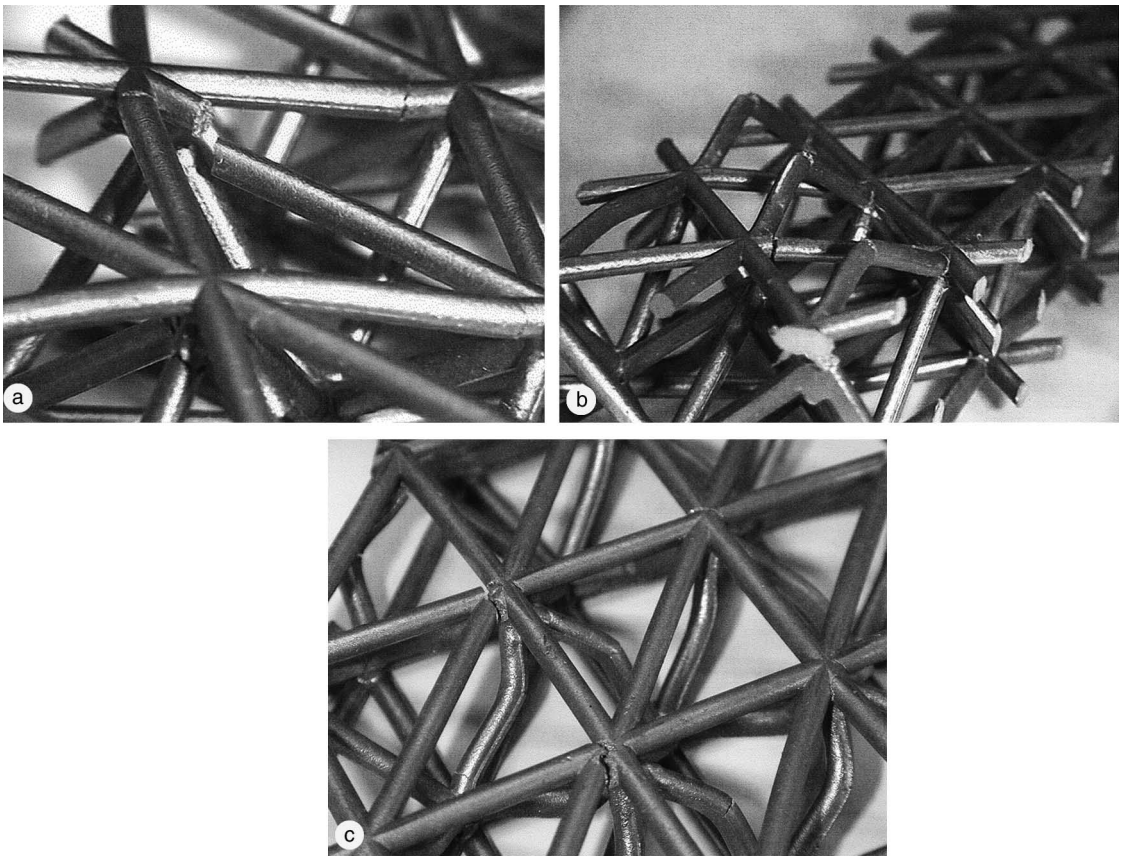

Fig. 10. Photographs of the failed specimens loaded in the (a) x (b) y and (c) z directions.

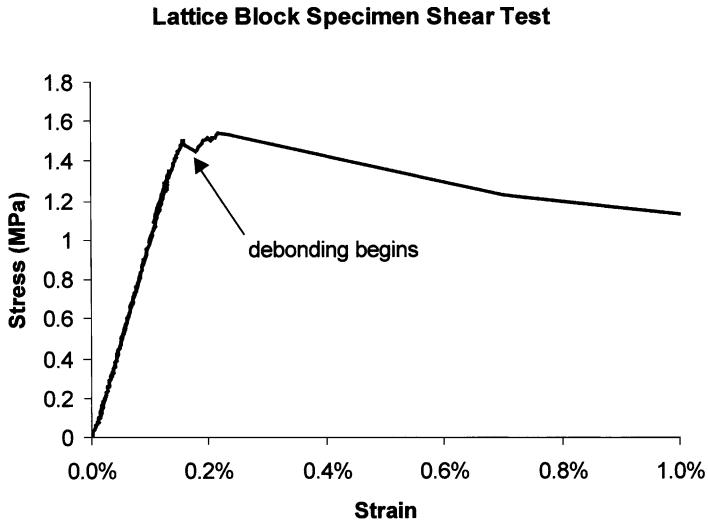

Fig. 11. Measured shear stress–strain curve for loading in the x–z plane.

Table 1
Comparison of predicted and experimental elastic properties

	Measured (GPa)	Calculated (GPa)	% error	2D periodic value (GPa) $\rho^*/\rho_s = 14.2\%$	3D periodic value (GPa)[a] $\rho^*/\rho_s = 9.89\%$
E_x	1.13[b]	0.96[b]	−15%	0.87	0.54
E_y	4.33[c]	4.45[c]	+3%	2.96	1.67
E_z	1.26[d]	1.35[e]	+7%	1.22	1.10
G_{xz}, G_{yz}	1.17[f]	0.92[g]	−27%	0.70	0.46
G_{xy}				0.89	0.43

[a] Calculations are based on models that do not include inner strut offset.
[b] Specimen was 5 cells × 1 cell, aligned along x direction.
[c] Specimen was 5 cells × 1 cell, aligned along y direction.
[d] Specimen was 1.5 cells (x direction) × 2 cells (y direction).
[e] Average from two models: a 1 cell × 2 cells model and a 2 cells × 2 cells model.
[f] Shear specimens were 8.5 cells × 1.5 cells. Two were tested with the long axis along the x direction, and two were tested with the long axis along the y direction. Results were the same within scatter, as predicated by symmetry.
[g] Average from two models: an 8 cells × 1 cell and a 9 cells × 2 cells model.

The model also predicts the nonlinear stress–strain response of the truss material. Results from three tests of x direction compression are plotted together with model results in Fig. 12. This model includes a random distortion to node positions to capture random variations in specimen geometry and material response. The model gives a good description of the measured compressive stress–strain curve. Results from tests of y direction compression agree equally well during linear loading and yielding, but the model underestimates failure stress. The elastic-hardening model (without material failure) gives a good description

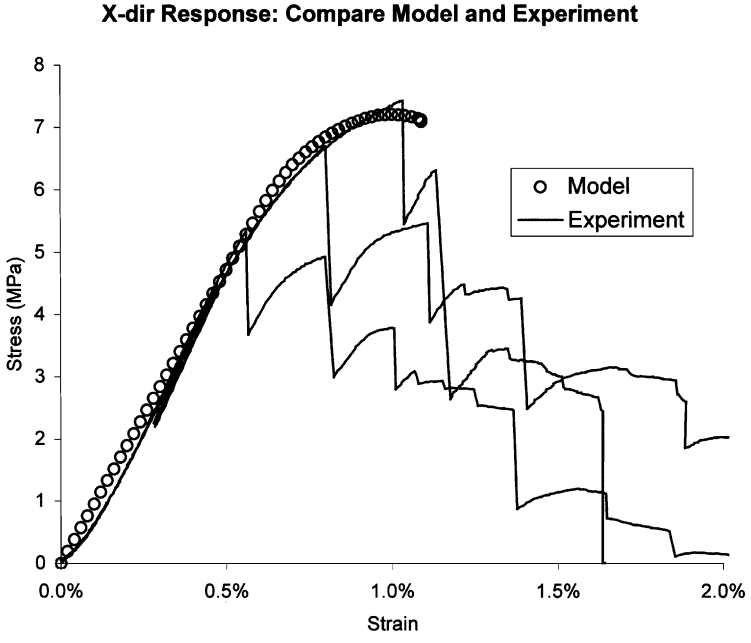

Fig. 12. Comparison of the measured and predicted stress–strain curve for the truss material for loading in the x direction.

Table 2
Failure stress for lattice block material, model and experiment

	Experiment (MPa)	Model (MPa)[a]	Model ( )/experiment
σ_x^*	6.50	8.03 (7.28)	1.12
σ_y^*	18.31	15.11 (14.72)	0.80
σ_z^*	9.01	8.92 (8.42)	0.93

Specimen sizes: x and y direction specimens were 5 cells × 1 cell. The z direction specimens were 2 cells × 4 cells.

[a] Two values for each model are given. The first is for a geometrically perfect model, and the (second) is for a model that includes random distortions in initial node position.

of the stress–strain curve up until failure. The measured strengths for loading in the x, y and z directions are compared with the model results in Table 2. The model predicts σ_x^* and σ_z^* well, but underestimates σ_y^*.

The larger discrepancy in $\sigma_{|y}^*$ may be understood by considering possible failure modes for individual members: yield and brittle failure in tension, yield and brittle failure in compression, and buckling. The model uses simple truss elements, and therefore captures only tension and compression failures. Buckling, which is physically possible, is neglected entirely in the simple model.

Some insight into actual failure mechanisms is gained by considering relative stresses in the linear elastic model. Relative stresses in individual members, which are calculated by normalizing the maximum member stress, are displayed for x, y, and z direction loading in Fig. 13. Specimens loaded in the x direction exhibit the largest stress and strain in face members loaded in compression. These members probably yield first, in compression, leading to increased strain in surrounding members. Tensile member stress and strain increase for compatibility, eventually leading to tensile member fracture. Finally compressive members bend and begin to crack on the tensile side. Specimens loaded in the y direction exhibit the largest stress in compression face members located parallel to the y direction. These members run continuously through the specimen in the y direction. Probably these members yield in compression and then buckle plastically during failure. Specimens loaded in the z direction exhibit the largest stress in core members running between the upper and lower faces. Probably these yield in compression, and eventually buckle plastically. In addition, there is tensile fracture in the most highly loaded tensile members on the faces.

As shown in Fig. 8, the material is stronger in compression. It is therefore plausible that members in compression, fail by buckling, and support higher ultimate stress and strain than members in tension, which fail by brittle fracture. It seems reasonable that the x direction model is most accurate because members fail in tension, which is well captured by the tensile material response data and the truss analysis. The y direction model may be less accurate because members fail in compression (buckling), which is poorly captured by the tensile material response data and the truss analysis. The z direction model is somewhat more accurate because members fail in tension as well as compression, and the model captures the tensile failure mode.

For a unit cell loaded in compression, the ratio of maximum tensile stress to maximum compressive stress is: for loading in the x direction, 0.602; for loading in the y direction, 0.337; and for loading in the z direction, 0.347. Therefore tensile failure is most likely for loading in the x direction, and buckling is most likely for loading in the y direction. These predictions agree with the failures in Fig. 10.

Young's moduli, the shear moduli and the uniaxial compressive strengths of the truss material are compared with those of a commercially available, nearly isotropic, closed-cell metallic foam (trade name Alporas, Shinko Wire, Amagasaki, Japan) in Table 3. The relative densities of the two materials are within 6% of each other. The truss material has superior properties in all cases with the exception of Young's moduli for loading in the x and z directions. The shear moduli and the uniaxial compressive strengths of the truss material in all three directions are significantly higher than those for the metallic foam.

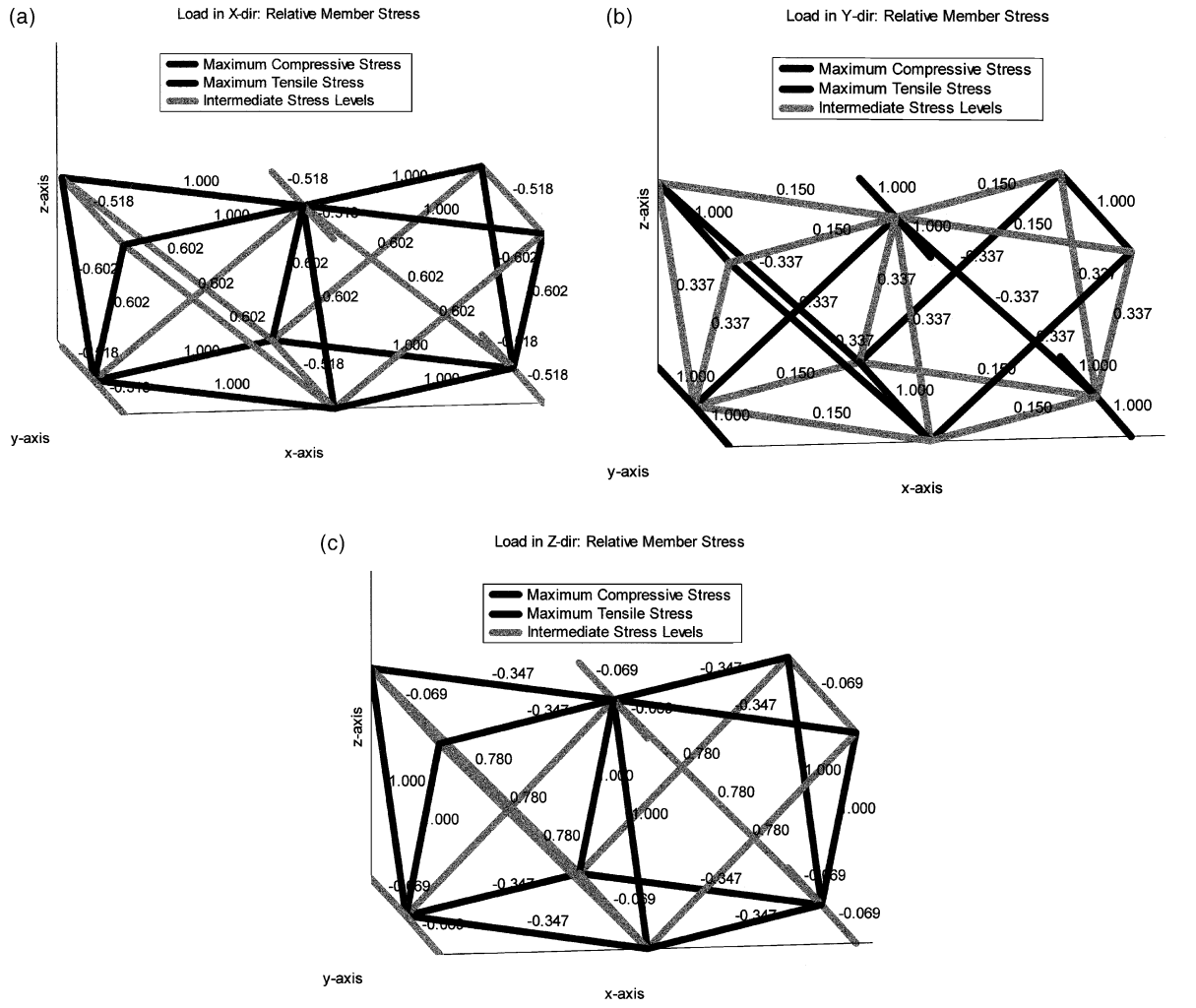

Fig. 13. Predicted member stress levels for a periodic truss material loaded in the (a) x- (b) y- and (c) z-directions. Member stress levels are normalized by the maximum member stress for each loading direction.

Table 3
Comparison of lattice block properties to those of Alulight, a metal foam

	Alulight	Lattice block[a]		
E_s (GPa)	69	69		
σ_{ys} (MPa)	250	224		
ρ^*/ρ_s	0.151	0.142		
		x direction	y direction	z direction
E^* (GPa)	1.68	1.13	4.33	1.26
σ^*_{ys} (MPa)	4.55	6.50	18.31	9.01
		G_{yz}	G_{xz}	G_{xy}
G^* (GPa)	0.63[b]	1.17	1.17	0.89 (est[c])

[a] Lattice block data are measured values, not model results.
[b] G for Alulight estimated assuming $v = 0.33$.
[c] G_{xy} was not measured for lattice block, so the model value is given.

7. Conclusions

The elastic moduli, the uniaxial compressive strengths and the shear strength of a 3D truss structure have been calculated in terms of the relative density of the structure, the aspect ratio and the properties of the solid from which it is made. The effect of sample size on Young's modulus has also been quantified. The calculated values of selected moduli and of the compressive strengths give a good description of the measured properties. The truss material has improved properties over commercially available closed-cell aluminum foams.

Acknowledgements

We gratefully acknowledge the financial support of ARPA through contract number N00014-96-1-1028. A graduate fellowship from the Fannie and John Hertz Foundation provided support for J.C. Wallach. We wish to thank Professor J.W. Hutchinson and Mr. Nathan Wicks of the Division of Engineering and Applied Sciences of Harvard University for several very helpful discussions. The truss material specimens were supplied by Jamcorp of Wilmington, MA.

References

ABAQUS Manual, Version 5.8. Hibbitt, Karlsson and Sorenson, Pawtucket, RI.

ASTM Standard C273-94, Standard test method for shear properties of sandwich core materials. American Society for Testing and Materials, 1994.

Davis, J.R. (Ed.), Aluminum and Aluminum Alloys. ASM Specialty Handbook. Menlo Park, ASM International, 1996.

MATLAB Manual, Version 5. The MathWorks, Inc., Natick, MA.

Weaver Jr., W., Gere, J., 1990. Matrix Analysis of Framed Structures, third ed. Van Nostrand Reinhold, New York.